Chapter 5

Bacterially Generated Nanocatalysts and Their Applications

Zhiyong Zheng,[1] Yong Xiao,[1,2] Feng Zhao,[2] Jens Ulstrup,[1] and Jingdong Zhang*[,1]

[1]Department of Chemistry, Technical University of Denmark, Kemitorvet, Building 207, DK-2800 Kongens Lyngby, Denmark

[2]CAS Key Laboratory of Urban Pollutant Conversion, Institute of Urban Environment, Chinese Academy of Sciences (CAS), 1799 Jimei Road, Xiamen 361021, China

***E-mail: jz@kemi.dtu.dk.**

Nanocatalysts synthesized by bacteria, mainly *Shewanella oneidensis* MR-1, are reviewed. Mechanisms of nanocatalyst biosynthesis by *S. oneidensis* MR-1, including intracellular and extracellular biosynthesis, are also discussed. We present characterization techniques such as UV-Vis spectroscopy, scanning electron microscopy (SEM), transmission electron microscopy (TEM), atomic force microscopy, X-ray photoelectron spectroscopy (XPS), X-ray diffraction (XRD), and thermogravimetric analyses. The biosynthesis process and information about a variety of resulting biogenic nanoparticle (NP) catalysts, particularly metallic and non-metallic NPs, alloys, and metallic and non-metallic sulfide NPs, are discussed further. Representative applications in electrocatalysis, photocatalysis, and biocatalysis are discussed, and opportunities and challenges of biogenic nanocatalysts are summarized.

Introduction

Nanomaterials have been defined as "materials with any external dimension in the nanoscale or having internal structure or surface structure in the nanoscale." "Nanoscale" is defined as a "length range approximately from 1 nm to 100 nm" (*1*). Nanocatalysts, therefore, refer to catalysts in the nanoscale. Compared to bulk counterparts, nanocatalysts offer a wealth of advantages, such as high activity, economy in atomic consumption, high selectivity, and stability. Due to these unique properties, nanocatalysts are attracting wide attention, and numerous nanocatalysts for a range of applications in clean energy technology and chemical industry have emerged.

Different methods to produce nanomaterials have been developed. Physical methods include ion implantation (*2*), vapor deposition (*3*), pulsed laser deposition (*4*), and mechanical techniques (*5*). The nanomaterials produced using physical methods are morphologically well controlled and environmentally friendly, but the methods are also limited by high complexity, low yield, and low efficiency (*6*). Chemical methods, such as ion exchange (*7*), sol-gel deposition (*8*), hydrothermal

Singh et al.; Novel Catalyst Materials for Bioelectrochemical Systems: Fundamentals and Applications
ACS Symposium Series; American Chemical Society: Washington, DC, 2020.

reactions (*9*, *10*), and chemical co-precipitation (*11*), produce high yields and can synthesize uniformly dispersive and narrow-sized nanomaterials in solution, but are demanding regarding experimental conditions, fraught by side reactions, and potentially harmful to the environment. Recently, green synthesis using non-toxic chemicals such as starch has emerged for platinum (*12*) and gold nanoparticles (NPs) (*13*).

The biosynthesis methods are eco-friendly and non-toxic. Different biological reactive agents react with metal ions and form corresponding NPs intra- or extracellularly (*14*). The biosynthesized nanomaterials also benefit from excellent biocompatibility, mild experimental conditions, low cost, high yield, and good scalability. The biosynthesis processes are very attractive because they can be accomplished using bacteria, fungi, plant extracts, and DNA (*15*, *16*).

Due to fast growth, low cost, and established genetic manipulation, bacterial biosynthesis of nanomaterials has been widely investigated. Bacterial biosynthesis of nanomaterials is simple and straightforward. Bacteria are cultured in nutritionally rich media (e.g., Luria broth) to obtain sufficient numbers of bacterial cells. The bacterial cells are then washed with water or a 0.9% NaCl aqueous solution to remove secretion. The cell pellet is then resuspended in a deoxygenated defined medium, such as M9 medium (*17*, *18*), 3-(N-morpholino)propanesulfonic acid buffer (*19*, *20*), sodium 4-(2-hydroxyethyl)-1-piperazineethanesulfonic acid (HEPES) buffer (*21–24*), a 0.9% NaCl aqueous solution, or even distilled water (*25*, *26*). Phosphate buffer solution, which is widely used in other applications of bioelectrochemical systems (*27*), is rarely chosen because most metal ions precipitate with phosphate. The redox properties of the medium should also be considered. Maintaining neutral pH is not essential since many bacteria can survive in high concentrations of metal ions due to the extracellular electron transfer (EET) process (*28*); for example, *Lysinibacillus* sp. ZYM-1 can produce Se NPs over a range of pH 5 to 9 (*29*). Finally, depending on nanomaterial and synthesis conditions (i.e. bacteria or medium), the target nanomaterials are synthesized within a few minutes, several hours, or even days after introducing metal ions into the medium (mainly as an electron acceptor) of specific bacteria.

Moreover, the biosynthesis process of nanomaterials by bacteria can achieve environmental remediation and material recycling at the same time. For example, *Cupriavidus necator* and *Pseudomonas putida* can remove Pd(II) from waste materials and the recycled Pd(0) nanomaterials were found to be able to catalyze Suzuki–Miyaura and Mizoroki–Heck reactions (*30*). The C-C bond formation was also catalyzed using the Pd(0) NPs produced by *C. necator* and *Cupriavidus metallidurans* from an acidic leachate containing several heavy metals including Pd(II) (*31*). The remediation by bacteria can be very efficient. *C. necator, P. putida,* and *Paracoccus denitrificans* removed 80%, 100%, and 100% of Pd(II), respectively. The Pd(0) nanomaterials obtained catalyzes dihydrogen production from hypophosphite (*32*).

Depending on extracellular or intracellular biosynthesis, different separation methods (e.g., centrifugation, sonication, and freeze-thawing) can be employed to obtain the separated nanomaterials (*33*). Separation of nanomaterials from bacterial cells is not generally required. Nanomaterial-bacteria hybrids offer several advantages compared to the separated nanomaterials. Aggregation is avoided in biosynthesized nanomaterials. Aggregation of nanomaterials has been a problem in applications, and different surfactants or stabilizing agents (e.g., polyethylene glycol) are used to solve the problem. However, the addition of surfactants often contributes to the decreased performance of the nanomaterials. Bacterial cells act as a supporter and framework in nanomaterial-bacteria hybrids, in which the formation sites for nanomaterials are uniformly distributed on the bacterial cell surfaces (e.g., the outer cell membrane) to efficiently prevent aggregation in this way.

Additionally, yield is increased compared to the separated nanomaterials. For small-sized NP materials (e.g., quantum dots), it is a challenge to retain samples during concentration and purification without aggregation. In contrast, nanomaterials generated by bacteria are attached on or enclosed in the cells. Concentration and purification can thus be accomplished straightforwardly by centrifugation. Other functions are also introduced via chemical doping elements. The main elemental composition of bacterial cells includes carbon (C), hydrogen (H), oxygen (O), nitrogen (N), phosphorus (P), and sulfur (S), in which N, P, and S are essential doping elements for catalysts. These elements can be doped into the nanomaterials in subsequent processes (*17*). After the formation of the nanomaterials, obtained or separated nanomaterials from the nanomaterial-bacteria hybrids can be used as electrocatalysts (*34*) in biosensors (*35*) and in electrosynthesis (*36*, *37*) as adsorbents (*24*) and as photothermal agents (*23*) without further treatment. In addition, further treatment (e.g., carbonization, hydrothermal processing, and microwave heating) can be implemented to enhance the electroconductivity and structure of the nanomaterials.

A variety of bacteria have been employed in the biosynthesis of nanomaterials, including *Saccharomyces cerevisiae* (*38*), *Bacillus subtilis* (*39*), *Shewanella* spp. (*17*, *25*, *34*), and *Escherichia coli* (*40*). As one of several models of electrochemically active bacteria (EAB) in bioelectrochemical systems, *Shewanella oneidensis* MR-1 has gained particular attention in the biosynthesis of various nanomaterials, including metal, metalloid, and inorganic compounds.

Shewanella was first classified in 1931 as belonging to the *Achromobacter* genus (*41*). Several reclassifications were conducted, and in 1985, the new name *Shewanella* was assigned to the genus to honor Dr. James M. Shewan's prolific contributions in fishery microbiology (*42*). *S. oneidensis* MR-1 was first discovered in Oneida Lake, New York in 1988 in relation to Mn^{4+} reduction and named as *Alteromonas putrefaciens* MR-1 (*43*). This bacterium was renamed as *Shewanella putrefaciens* MR-1 before finally being named *S. oneidensis* MR-1 after the lake where it was discovered (*44*). The term "MR" is the abbreviation for "manganese reducer".

S. oneidensis MR-1 is a facultatively aerobic Gram-negative bacterium (*45*), approximately 2–3 μm in length and 0.5 μm across (Figure 1). As a dissimilatory metal-reducing bacterium, *S. oneidensis* MR-1 can anaerobically reduce various metal ions such as Au(III) (*25*), Pd(II) (*18*, *34*), Pt(IV) (*17*), and Ag(I) (*46*), to form the corresponding metallic nanomaterials. The metal ions are electron acceptors in bacterial biosynthesis. This process correlates with the EET process (Figure 2), in which EAB exchange electrons with external redox partners, electrochemical electrodes, or other EAB through one of three different pathways (*47*, *48*). The first pathway is short-range direct EET, in which EAB exchange electrons with external redox partners via redox proteins in the outer cell membrane, such as OmcA and MtrC. The second pathway is long-range direct EET. *S. oneidensis* MR-1 develops conductive appendices (also termed as "pili" or "nanowires") to reach redox partners when nutrients are limited. The final pathway is mediated EET, in which *S. oneidensis* MR-1 secretes redox mediators (e.g., flavins) to shuttle EET. This pathway dominates the EET process of *S. oneidensis* MR-1 and contributes more than 70% of the EET (*49*–*52*). In all the pathways, the electrons are transferred by "hoping" in extracellular polymeric substances (EPSs), which envelop the bacteria (*49*).

Much attention has been given to the biosynthesis of nanomaterials, and several studies have summarized these developments (*53*–*59*). The present chapter provides a general view of metallic and non-metallic nanocatalysts synthesized by bacteria. In particular, the mechanism of bacterial NP biosynthesis with focus on *S. oneidensis* MR-1 is discussed. Characterization methods of the

catalytic NPs are described, their applications are summarized, and new prospects and challenges of biosynthesized nanocatalysts are envisioned.

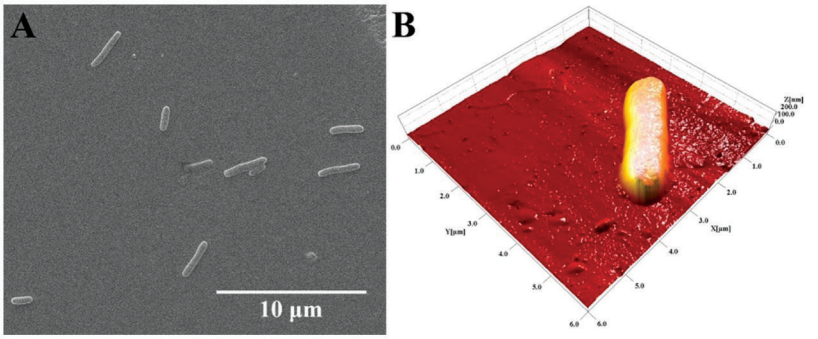

Figure 1. Morphology of S. oneidensis MR-1. (A) Scanning electron microscopy (SEM) and (B) atomic force microscopy (AFM) images of S. oneidensis MR-1.

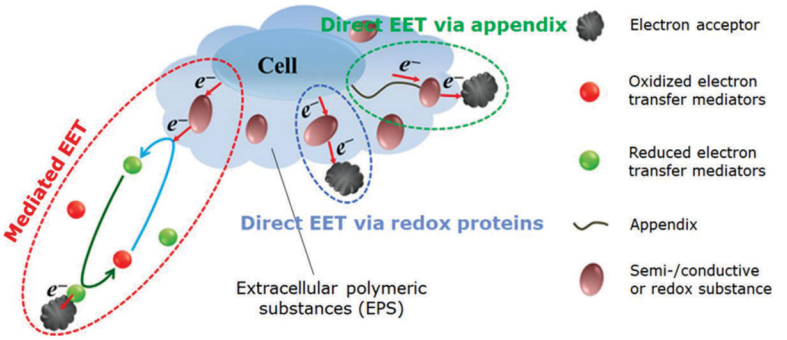

Figure 2. Three pathways of EET of S. oneidensis MR-1. Adapted with permission from reference (49). Copyright 2016 the American Association for the Advancement of Science.

Biosynthesis Mechanisms of Nanocatalysts

Metal ions and metal complexes are often positively charged while there are numerous negatively charged sites on the bacterial cell membrane due to the presence of glycoconjugates and surface groups such as carboxylate groups (*60*, *61*). There are, however, also positively charged sites on the cell surface caused by positively charged proteins, which attract negatively charged metal complexes. As shown in Figure 3, target ions are captured from the environment by electrostatic interactions. The ions are then extracellularly converted into elemental metals by redox molecules on the outer membrane (e.g., cytochromes and enzymes). Alternatively, the ions are transported through the outer membrane, interact with redox molecules, and intracellularly transformed into nanocatalysts in the periplasm (*19*, *25*, *34*, *60*, *62*).

The exact routes for bacterial nanocatalyst biosynthesis are very complex and vary depending on the bacteria and ions. Presently, focus is on the mechanism of bacterial biosynthesis of nanocatalysts by the representative bacterium (*S. oneidensis* MR-1). This bacterium can reduce a variety of metal ions and EET of this particular species has been well studied.

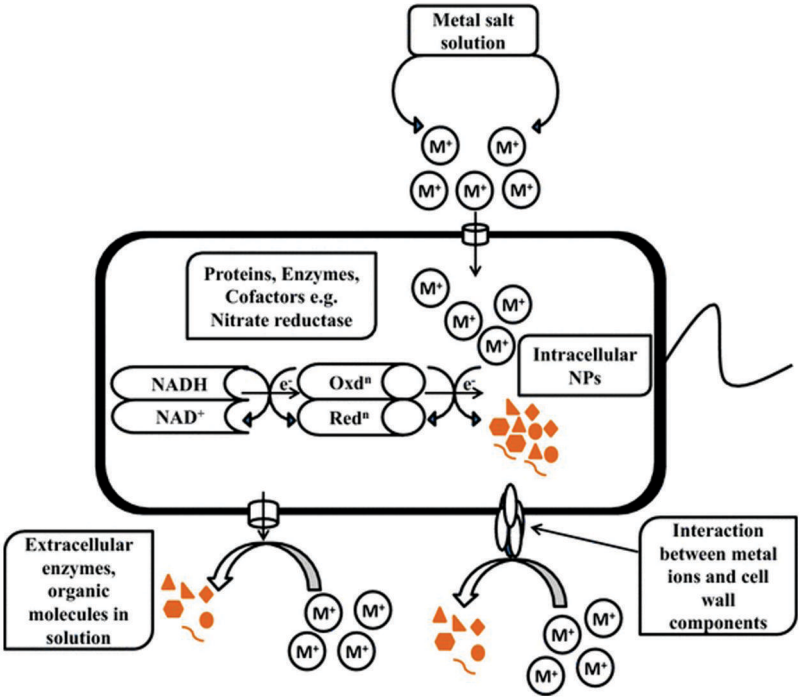

Figure 3. Microbial synthesis mechanism of nanocatalysts. Adapted with permission from reference (*60*). *Copyright 2016 Springer Nature.*

The cell membrane of *S. oneidensis* MR-1 is shown schematically in Figure 4. The formation of nanocatalysts correlates with the precipitation and bioreduction of metal ions by EAB (*63*). Metal ions precipitate on or within the bacterial cell because the metal concentration exceeds the stoichiometry per reactive sites on or in the cell. That means that a small amount of soluble metals can be associated with cell surface or inside the cell, while high metal concentration can cause precipitation on the reactive sites (*64*). Although three EET pathways for *S. oneidensis* MR-1 have been proposed, the short-range direct EET prevails in the biosynthesis of nanocatalysts compared to the other two pathways. Nanowires are unlikely to be formed in the biosynthesis, in which abundant metal ions are present as electron acceptors and are usually formed only when electron acceptors are limited (*65*). In the mediated EET pathway, *S. oneidensis* MR-1 excretes flavins, which mediate the EET between the cells and external electron acceptors (*52*). However, biosynthesis of nanocatalysts by flavins is hampered since their midpoint potentials are in the range -0.2 to -0.25 V compared to the standard hydrogen electrode (*52*). Different cytochromes *c* (e.g., MtrC, MtrA, and OmcA) are involved in the short-range direct EET and form the OmcA–MtrCAB pathway (*49*, *66*). Electrons from oxidized quinol are first delivered to CymA, where the electrons are then carried to MtrA using FccA and a small tetraheme cytochrome (STC). This is followed by electron transport successively through MtrA, MtrB, and MtrC, which constitutes a complex penetrating the outer cell membrane. Finally, outer membrane cytochromes *c* MtrC and OmcA directly relay the electrons to metal ions (*67*–*69*). MtrA and OmcA are therefore important for the biosynthesis of metallic nanocatalysts and strongly affect the size of the nanocatalyst particles (*20*). Nonetheless, the presence of MtrA and OmcA is not indispensable for the formation of all nanomaterials since a mutant without MtrA and OmcA (*S. oneidensis* MR-1 *ΔomcA/mtrC*) can also synthesize nanocatalysts such as Ag (*20*), Se(IV) (*21*), and Au (*25*) NPs. The nanocatalysts synthesized by the mutant can differ in size and

antibacterial activity from those synthesized by the wildtype, making controlling synthesis by gene technologies possible (*20*). The ability of *S. oneidensis* MR-1 *ΔomcA/mtrC* to synthesize extracellular nanocatalysts indicates that other reactive sites are present, but the details regarding these sites remain to be explored.

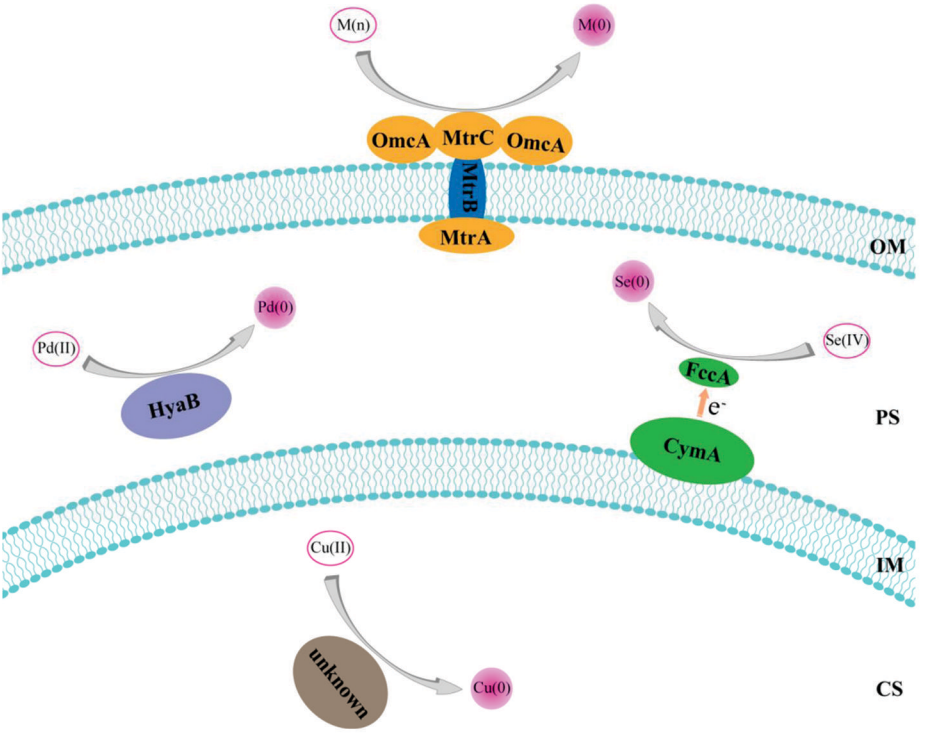

Figure 4. Schematic view of cell membrane structure of S. oneidensis MR-1 and main synthesis sites of metallic and metalloid nanomaterials. M(n) = Tc(VII), Ag(I), U(VI), and Au(III). OM: outer membrane; PS: periplasm; IM: inner membrane; CS: cytoplasm. Note that the indicated sites are the primary sites for the metals and metalloids, but other sites are also possible. For simplicity, the quinol and other structures are not presented.

Moreover, some studies show that MtrC and OmcA play an important role in the reduction of Fe(III), Cr(VI), Tc(VII), Ag(I), Au(III), and U(VI) (*20*, *28*, *70*, *71*), while other studies imply that hydrogenases, specifically [NiFe]-hydrogenase HyaB, are responsible for the reduction of Pd(II) (*22*). Two main hydrogenases are present in the genome of *S. oneidensis* MR-1: HydA and HyaB (*72*). HydA is a periplasmic [Fe-Fe] hydrogenase, which is involved in dihydrogen formation, while HyaB is a bifunctional periplasmic [Ni-Fe] hydrogenase responsible for either the formation or oxidation of dihydrogen (*72*). The Pd(II) complex, normally $[PdCl_4]^{2-}$, has to penetrate the outer cell membrane in order to be reduced by HyaB, but only limited information about the mechanism of how $[PdCl_4]^{2-}$ is transported through the outer membrane is available. On the other hand, abundant Pd NPs were also found on the outer membrane (*34*).

The OmcA-MtrCAB pathway, nitrate and nitrite reductase, and hydrogenase are reported to have little effect on the reduction of SeO_3^{2-} to Se(0). In the periplasm, CymA relays electrons from quinol to fumarate reductase FccA, which further reduces SeO_3^{2-} to Se(0) (*21*). Different from

Au, Pd, or Pt NPs with uniform and small size, the Se NPs are apparently bigger and more widely dispersed in size.

Apart from the formation of nanocatalysts in the outer membrane and the periplasm of *S. oneidensis* MR-1, Cu particles are also found to be dispersed in the cytoplasm and periplasm. In the reduction of Cu(II), MtrC, OmcA, MtrF, MtrABCDEF, DmsE, S04360, and CctA did not play a key role. The reduction of Cu(II) could happen intracellularly, with possible unidentified reductases involved (*19*). Tellurium (Te) nanomaterials were also observed in the cytoplasm and periplasm (*73*, *74*), but detailed mechanisms are not clear.

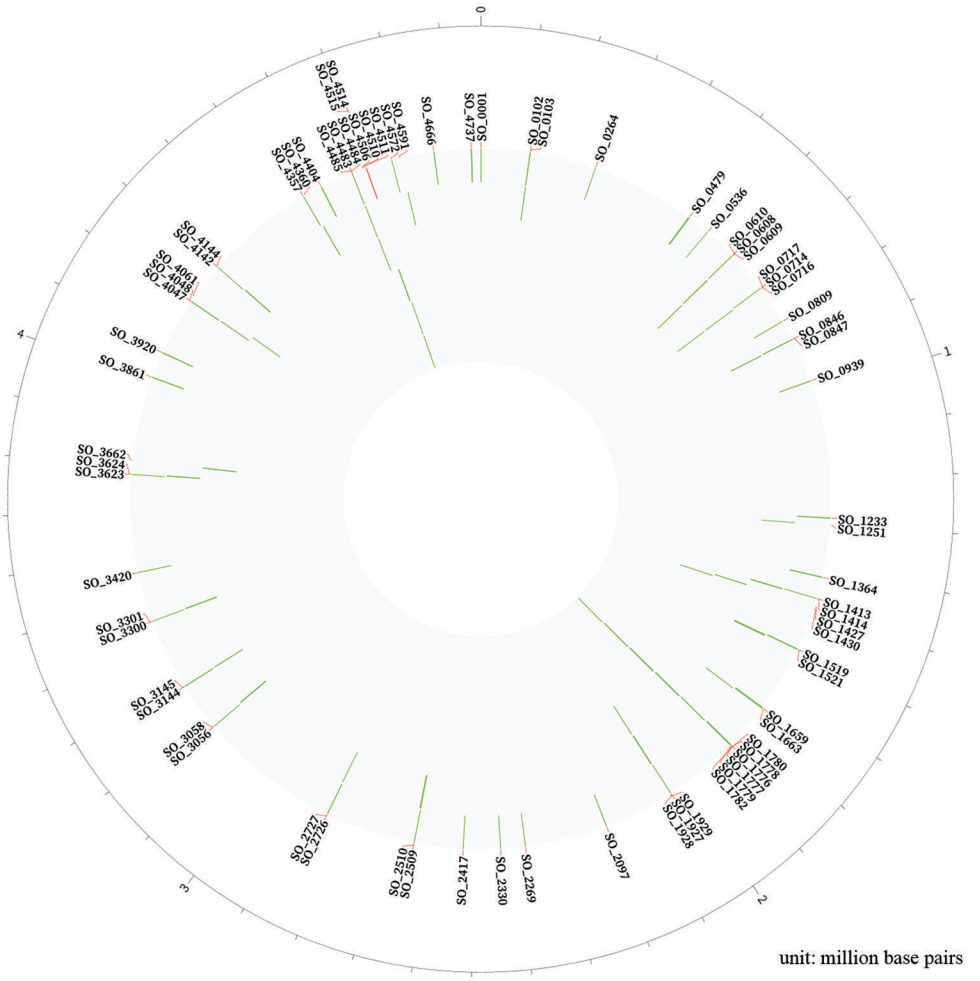

Figure 5. Circular representation of the S. oneidensis MR-1 chromosome sequence related to EET process. The sequence originates from GenBank (accession numbers AE014299).

The genome of *S. oneidensis* MR-1 is composed of 4,969,803 base pairs (*45*), including 76 base pairs involving the EET process according to information from the National Center for Biotechnology Information database (Figure 5). Products of the 76 include cytochromes, hydrogenases, reductases, and flavodoxins, among others. It has been reported that there are 39 cythchromes *c* in *S. oneidensis* MR-1 including 8 decaheme cytochrome *c* (*45*). The vital genes in the OmcA–MtrCAB pathway are summarized in Table 1. Note that among the 39 cytochromes *c*, only 6 of them (MtrA, MtrC, OmcA, CymA, small tetraheme cytochrome, and FccA) have been

well documented in the EET process, and even fewer have been fully investigated in the synthesis of nanomaterials.

Table 1. Important Genes in OmcA-MtrCAB Pathway

Locus tag	*No. of Haems*	*Location in the Cell*	*Reference for S. oneidensis MR-1*
SO_1776	-[a]	Outer membrane	MtrB
SO_1777	10	Periplasm	MtrA
SO_1778	10	Outer membrane	MtrC
SO_1779	10	Outer membrane	OmcA
SO_4591	4	Periplasm	CymA

[a] MtrB is not a cytochrome *c* and contains no haem.

In summary, various electron transport pathways in *S. oneidensis* MR-1 provide different biosynthesis mechanisms. Different enzymes and 42 cytochrome *c* species are present in the genome of the bacteria, but only some of them have been studied (e.g., MtrC, OmcA, MtrB, CymA). The three established EET pathways dominate the reduction of insoluble Mn(IV) and Fe(III) (hydro)oxides, but different EET processes operate for other soluble metal ions (Figure 4).

Characterization of Biogenic Nanocatalysts

In the bacterial synthesis of nanocatalysts, it is important to follow the formation process. The defined medium changes to pale yellow after bacterial cells (e.g., *S. oneidensis* MR-1) are resuspended into the medium. The medium can change to a specific color or the color of the metal ions fade as the nanocatalysts are formed, which means that the formation of some nanocatalysts can be followed directly with UV-Vis spectroscopy. For example, the absorption peak around the wavelength of maximum absorbance (λ_{max}) of 411 nm disappears when Pd nanocatalysts are formed (*34*). A peak at $\lambda_{max} = 530$ nm appears within 24 h in the biosynthesis of Au nanomaterial using *S. oneidensis* MR-1 (*28*). For Ag nanomaterials, a peak at $\lambda_{max} = 418$ nm emerges in the colorless $AgNO_3$ solution containing *S. oneidensis* MR-1 after 48 h (*46*). CuS NPs form simultaneously with the appearance of a peak at $\lambda_{max} = 1100$ nm (*23*). Moreover, since λ_{max} is strongly linked with the size or the structure of nanomaterials, the evolution of nanomaterials can be monitored by UV-Vis spectroscopy. For example, a spectral red shift indicates an increasing amount of CdS quantum dots (*38*).

Electron microscopy technologies are crucial for visualization of the precise size and morphology as well as the structure of the nanocatalyst NPs. The most common of these technologies are SEM and TEM. The SEM and TEM sample preparations are similar, and fixation (usually by glutaraldehyde) and dehydration (e.g., gradient ethanol dehydration) are required to maintain the original structure of the bacterial cells (*17*, *34*, *38*, *75*). A relatively low voltage (5–20 kV) is applied in SEM of biological samples to avoid destroying the samples (*76*). SEM can image a large enough area for nanomaterial-bacteria hybrids, and the resolution can reach 1 nm. The diameter of bacterial cells can be several hundred nanometers, but slicing is not required if the inside structure of the cells is not addressed. Advanced SEM technologies have emerged and provided much more information. For example, "3D" images were constructed with serial block-face SEM, confirming the presence of Cu NPs inside the *S. oneidensis* MR-1 cells (*19*). TEM is very powerful for observing both the morphology and structure of the nanomaterials, but ultra-thin sections of the nanomaterial-

bacterial hybrids must be sliced if the inside of the cells is to be mapped (*19*, *25*) since the electron beam of the TEM cannot penetrate samples thicker than 100 nm. The surface facets of the nanocatalysts are key factors for their performance, and the extraordinary nanometer-to-atomic TEM resolution makes the acquisition of such information possible, particularly the structure of the crystal lattice (*17*, *23*). Coupled with energy-dispersive X-ray spectroscopy (EDS), TEM can map not only the morphology of the nanocatalysts, but also the elemental composition, which is essential for the characterization of alloys and core-shell NPs. For example, the EDS mapping displayed in Figure 6 shows clearly overlapping Pd, Au, P, and S peaks, indicative of a doped alloy (*17*).

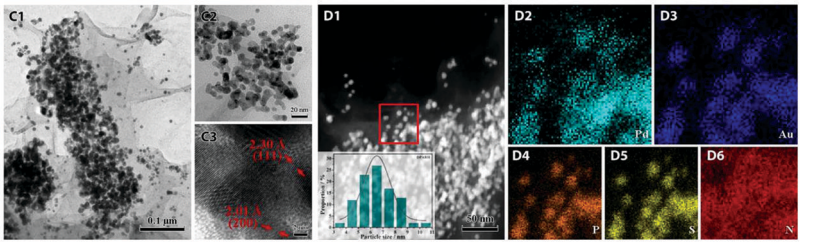

Figure 6. TEM and corresponding EDS mapping of PdAu alloy biosynthesized by S. oneidensis MR-1 with subsequent hydrothermal treatment. Reproduced with permission from reference (*17*). *Copyright 2016 the American Association for the Advancement of Science.*

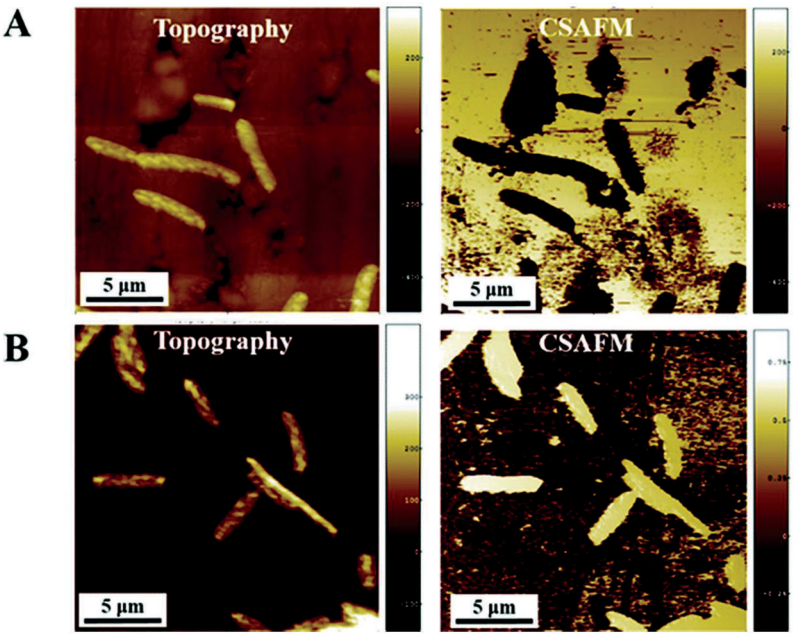

Figure 7. Representative topographic (left) and current-sensing AFM images (right) of (A) S. oneidensis MR-1 and (B) S. oneidensis MR-1 coated with biosynthesized Pd nanocatalysts. Reproduced with permission from reference (*34*). *Copyright 2018 The Royal Society of Chemistry.*

Another versatile technique is AFM. The resolution of AFM can also reach the nanometer level, and, AFM is therefore suitable for precise imaging of nanomaterials (*46*). The sample preparation of AFM is simple with a small number of samples immobilized and spread out on a flat surface. Fixation, dehydration, coating with metal layer, and slicing are not needed, which minimizes sample destruction. There is no need for a vacuum; AFM can be conducted in ambient atmosphere and even

in solution. In addition, 3D images can be readily constructed from AFM measurements (Figure 1A). AFM can provide physical properties and information other than size and morphology. For instance, Figure 7 shows a comparison between the topographic and current-sensing AFM (CSAFM) images of *S. oneidensis* MR-1 cells coated with Pd NPs that are apparently different from pristine *S. oneidensis* MR-1 cells. Compared with the dark area in pristine *S. oneidensis* MR-1 cells, the brightness of the cells coated with biosynthesized Pd nanocatalysts reflects higher conductivity, since the brightness in CSAFM images indicates the current flow between the AFM tip and the substrate (*34*).

EDS in SEM and TEM can show the elemental composition but does not give other information, such as chemical and electronic state of the elements. X-ray photoelectron spectroscopy (XPS) is helpful in achieving this additional information. XPS is a qualitative and semiquantitative analysis method for chemical surface elements including the chemical and electronic states. For example, a peak belonging to Se_{3d} emerged in Se nanospheres synthesized by MR-1 (*35*). In another study, the ratio of Pd, Au, P, N, and S elements (32.28:10.83:4.32:47.09:5.48) was obtained using XPS (*17*).

The qualitative and semiquantitative information from XPS analysis is highly valuable, but XPS is limited only to the surface of the sample (e.g., 20 nm into samples). This is not comprehensive enough for bulk materials (i.e. nanomaterial-bacterial hybrids), which are hundreds of nanometers in diameter. To get the crystal structure on or within nanomaterial-bacterial hybrids, X-ray diffraction (XRD) analysis, in which the penetration of the X-ray can be several millimeters, is practical. For example, both peaks belonging to Au and Pd were observed in the PdAu alloy (*17*, *26*). Nonetheless, XRD analysis alone is not sufficient to confirm the phase analysis since the XRD pattern of different crystals can be very similar and it is difficult to analyze when different crystals co-exist. Moreover, signals are weak if the nanocatalysts are amorphous or the metals are highly dispersed in the nanomaterials. If possible, XRD, EDS, TEM, and XPS analysis should all be considered (*17*, *23*).

The biosynthesized nanocatalysts are different from their chemically synthesized analogues. Bacterial cells are normally covered with EPS, and organic substances can participate in the formation of the nanocatalysts. To quantify these substances, thermogravimetric analyses can be employed. For example, the weight loss from 100 to 400 °C is caused by thermal decomposition of adsorbed organic substances in nanomaterials synthesized by bacteria, while the weight loss from 400 to 800 °C is due to decomposition of intracrystalline organic substances (*26*, *77*).

Classes of Biogenic Nanocatalysts

Metals and Alloys

Much attention has been given to the biosynthesis of metallic nanomaterials, (especially noble metal nanomaterials) due to the considerable economic benefits of metal recovery (*54*). A variety of noble metal ions, such as Au(III), Pt(IV), Pd(III), and Ag(I), can be recovered by bacteria (*17*, *46*, *78*, *79*). The local size of the nanomaterials depends on experimental conditions, but typically the microstructures of noble metal nanomaterials are small (i.e., in ranges from a few to tens of nanometers) and uniform. Biogenic Pt NPs synthesized by *Shewanella algae* (*79*) are about 5 nm. Au and Pd NPs synthesized by *S. oneidensis* MR-1 are 5–30 nm (*25*) and 3–10 nm (*34*), respectively. The size of Ag NPs is similar to that of Pd NPs (i.e., about 2–10 nm in diameter) (*46*).

The recovery of noble metal ions is very high within a relatively short treatment time. For example, a recovery of 99.6% of Pd(II) was achieved by *S. oneidensis* MR-1 ($OD_{600} = 2.0$) overnight

when 50 mg/L of Pd(II) was used as an electron acceptor and dihydrogen as an electron donor (*18*). The recovery remains high at high concentrations of Pd(II). For instance, only 0.1 mg/L remained in the solution when 1000 mg/L of Pd(II) was introduced (*18*). Au (III) removal can be visually observed within 30 min indicated by the color change from pale yellow to purple when *S. oneidensis* MR-1 is exposed to 100 mg/L of $[AuCl_4]^-$ (*25*). Similarly, about 90% of $[PtCl_6]^{2-}$ was removed by *S. algae* in 60 min (*79*).

Other metal ions can also be recovered by bacteria, forming corresponding metal NPs. The Cu NPs synthesized by *S. oneidensis* MR-1 are relatively larger than the noble metal NPs just noted, with a typical size range of 20 to 40 nm (*19*). The recovery of Cu(II) is also high, with 70% after 3 h, 91% after 24 h, and 100% after 96 h. The core of the NPs is Cu(0), while the surface is Cu_2O due to oxidation caused by exposure to oxygen in the air (*19*). Co NPs of 4-8 nm in length were formed in the outer membrane of *S. putrefaciens* CN32 after the cells were exposed to 195 mg/L of Co^{2+} in pH 3 for 24 h. Moderate recovery of 21% was achieved with an initial concentration of 210.745 mg/L. The limited recovery may be due to the short lifespan of the bacteria under these experimental conditions (*80*).

The ability of EAB to reduce various metal ions offers an approach for the synthesis of alloys. A highly dispersed PdAu alloy was synthesized on the cell surface of *S. oneidensis* MR-1 after successive addition of $[AuCl_4]^-$ and $[PdCl_4]^{2-}$. As shown in Figure 6, NPs of this alloy are quite small, with an average diameter of 5 nm (*17*). An extracellular PdAu alloy is also formed when a higher concentration of $[PdCl_4]^{2-}$ and $[AuCl_4]^-$ are used as electron acceptors; for example, a nanocomposite of PdAu alloy and Fe_3O_4 with an NP size of 3–15 nm was obtained from *S. oneidensis* MR-1 after 1 mM of $[PdCl_4]^{2-}$ and 1 mM of $[AuCl_4]^-$ were introduced into the medium containing akaganeite for 48 h (*26*).

Metal and Metalloid Sulfides

EAB can also reduce sulfur and thiosulfate to sulfide (*81*), producing metal sulfides when specific metal ions, sulfur, and thiosulfate as electron acceptors are present simultaneously. For example, brown-colored CuS NPs with a uniform size of about 5 nm are formed extracellularly, when *S. oneidensis* MR-1 is incubated in a HEPES-buffered mineral medium containing 1 mM of $Na_2S_2O_3$, $CuCl_2$, and 20 mM of lactate. The Cu:S ratio was 0.94:1 analyzed from XPS results (*23*). In another study, CuS nanorods with 17.4 nm and 80.8 nm in diameter and length were embedded in the *S. oneidensis* MR-1 cell membrane, forming a complex hollow shell structure (*24*).

S. oneidensis MR-1 can synthesize Ag_2S NPs of 53.4 $\pm$ 12.4 nm. The size of the NPs decreased to 27.6$\pm$ 6.4 nm when MtrC and OmcA were knocked out (*20*). In contrast, another study showed that the presence of *S. oneidensis* MR-1 cells is not required to form Ag_2S NPs (*82*). These authors inferred that the complex $Na_3[Ag(S_2O_3)_2]$ caused precipitation of Ag_2S. However, MtrC, OmcA, and MtrB from *S. oneidensis* MR-1 can stabilize Ag_2S NPs. The native cell structure stabilizes rather than forms Ag_2S NPs, which means larger Ag_2S NPs are formed in the absence of *S. oneidensis* MR-1 cells (*82*). Smaller Ag_2S NPs can also be obtained from the same bacterium. For example, Ag_2S NPs smaller than 8 nm attached to TiO_2 nanotubes have been produced by *S. oneidensis* MR-1 (*83*).

FeS can also be formed abiotically. For example, poorly crystalline FeS can be obtained by mixing 0.57 M of $FeCl_2$ and 1.1 M of Na_2S (*84*). Different from abiotic FeS with bulk and irregular forms, the biogenic FeS synthesized by *S. putrefaciens* CN32 is mainly comprised of 100-nm NPs. Moreover, the biogenic Fe:S ratio was 2.3, which is different from that of abiotic FeS with a ratio of 1.3 (*85*).

CdS NPs ("quantum dots") with an average diameter of 2 nm can be synthesized by *S. cerevisiae* via yeast cells cultured in 0.1 mM of $CdCl_2$ and 0.05 mM of Na_2S for one day. Notably, the size of the CdS quantum dots increases with longer culture times (*38*). Much larger CdS NPs (about 15 nm in diameter) synthesized by *S. oneidensis* MR-1 have also been reported (*86*). Moreover, the addition of ionic liquid can modify the CdS NPs from agglomerated and irregular shapes to highly ordered spherical structures (*86*).

Biosynthesis also provides morphologies that are not available from chemical synthesis. AsS nanotubes that are 20–100 nm in diameter and about 30 μm in length were produced extracellularly by *Shewanella* sp. strain HN-41 in a medium containing As(V) and $S_2O_3^{2-}$. The nanotube composition nine days after inoculation was As_2S_3, which transformed to AsS after two to three weeks (*87*).

Notably, the addition of metal and sulfur or thiosulfate is sometimes not needed. Some bacteria are able to synthesize metal sulfide-based nanomaterials even in groundwater. Natural biofilms of *Desulfobacteraceae* can, for example, synthesize 2–5-nm ZnS NPs by accumulating a Zn concentration that is 10^6 times over ground water level (*88*).

The biosynthesis of other metal sulfides is also reported, such as MnS (*89*), but the application of these metal sulfides as catalysts is rarely reported. We therefore do not include detailed discussion of these other biogenic metal sulfides.

Metal Oxides and Metal Hydroxides

Fe_3O_4 NPs were obtained under anaerobic conditions by transforming akaganeite to magnetite by culturing *S. oneidensis* MR-1 with lactate as an electron donor for 48 h. The Fe_3O_4 NP size was 3–15 nm in diameter (*26*). Larger Fe_3O_4 NPs with a diameter of 26–38 nm can be acquired from *Shewanella* sp. HN-41 using a similar method (*90*).

In contrast, another study reported that the transformation of akageneite by *Shewanella* sp. HN-41 depends on the amount of akaganeite precursors and Fe(II) in the solution. Akaganeite nanorods that are about 5 nm in width and 20 nm in length were used as precursors and electron acceptors. When 30-mM akaganeite was introduced after 10 days, magnetite NPs up to 100 nm diameter appeared. However, goethite nanowires 15 nm in width and 500 nm in length appeared instead (*91*).

UO_2 NPs formed when *S. oneidensis* MR-1 cells were inoculated in 250 μm of uranyl acetate and 10 mM of sodium lactate under anaerobic conditions. The UO_2 NPs are quite small, only 1–5 nm in diameter. The NPs appeared in three forms, in which some, densely packed with EPS, were complex structures, similar to glycocalyx. This indicates that EPS (possibly with a redox substance inside) plays an important role in the formation of UO_2 NPs (*71*).

Metalloids

Apart from metals and metal compounds, the biosynthesis of metalloid nanomaterials by EAB have been extensively studied (*92*). For example, the size distribution of Se NPs can be adjusted by controlling the biomass concentration of *Shewanella* sp. HN-41 and the initial selenite concentration. Within 2 h, 1–20 nm amorphous Se NPs were produced with low initial biomass under anaerobic conditions. Much larger NPs (about 150 nm) were also observed. Se NPs around 123 nm were produced when a larger initial biomass was exposed for 24 h (*93*). Different bacteria can synthesize Se NPs at different sizes using different mechanisms of Se(VI) reduction. Large, 100–250 nm Se NPs were synthesized by *S. oneidensis* MR-1, and smaller 50–100 nm Se NPs were acquired by *Geobacter sulfurreducens* (ATCC 51573), while the smallest Se NPs (around 50 nm) were synthesized by *Veillonella atypica* (ATCC 14894) (*94*). Another study showed that the bigger Se NPs (around 100 nm) formed inside the cells, while smaller Se NPs (around 20 nm) formed extracellularly; the biosynthesis of Se NPs is potentially controlled by the EPS (*21*).

Another metalloid NP biosynthesis by EAB was also reported (*63*). Tellurite (Te) nanomaterials were formed inside *S. oneidensis* MR-1, and a pathway different from Se reduction was proposed (*74*). According to another detailed study, more than 90% of Te(IV) was recovered after incubating *S. oneidensis* MR-1 in 100 μM of sodium Te and 10 mM sodium lactate for 120 h. The products are single-crystalline Te nanorods with a length of 100–200 nm (*73*). Notably, the presence of Fe(III) will change the synthesis location and the size of the Te nanorods. When Te(IV) and Fe(III) co-exist in the medium, more extracellular Te nanorods accumulated with 240 nm and 25 nm for the length and diameter, respectively. However, when Te(IV) was introduced after Fe(III) was reduced to Fe(II), exclusively extracellular crystalline Te nanorods were formed at a smaller size (i.e., 89 nm and 7.5 nm in the length and diameter, respectively were found) (*95*). In addition, *Shewanella baltica* was reported as having the ability to reduce Te(IV) and form 8–75 nm Te nanorods (*96*).

Applications of Biogenic Nanocatalysts

As noted, different bacteria can synthesize various nanomaterials . The resulting nanomaterials offer numerous applications. The applications of catalytic NPs synthesized by *S. oneidensis* MR-1 and other representative bacteria are summarized in Table 2. Three kinds of applications (i.e., electrocatalysts, photocatalysts, and biocatalysts) are discussed below.

Electrocatalysis

The biosynthesized nanocatalysts not only exhibit some exclusive morphology, but also unique catalytic properties. Pd NPs synthesized by *S. oneidensis* MR-1 show unique selective catalysis to formate electrooxidation, but no electrocatalysis to oxidize other biofuels, such as ethanol, methanol, and acetate, in neutral solution. The selectivity is caused by preferential binding of formate over the other fuels. Moreover, compared to Pd electrodeposited on an electrode, the anodic peak for formate oxidation is more negative by 220 mV (0.10 V vs. a saturated calomel electrode), and exhibit less activation energy (*34*). The poor conductivity of the cell substrate itself is compensated by the PdNP coating, as inferred clearly from the current-sensing AFM images (Figure 7).

EAB can also facilitate nanocatalyst formation not only on the cell surface, but also on electrochemical electrode surfaces. For example, 10–100 nm Pd NPs were coated on a cathode (a piece of carbon cloth) by *S. oneidensis* MR-1 poised at 0.8 V. The size increased to 200–250 nm for abiotic Pd NPs produced using electrochemical method. The smaller size of the NPs and the presence

of cells as biocatalysts led to a larger surface area, resulting 90.0 ± 1.4 Coulombs of electron transfer in dihydrogen production with a Pd loading of 40.5 m^2 g^{-1}. This is much higher than the 75.0 ± 1.2 Coulombs in the absence of the bacteria. As a result, the dihydrogen production and recovery (61.8 ± 2.0 L-H_2 m^{-3} day^{-1}, hydrogen volume per reactor volume per day, and 65.5 ± 3.1%, respectively) in the presence of the bacteria were significantly higher than in the absence of bacteria (38.5 ± 2.0 L-H_2 m^{-3} day^{-1} and 47.3 ± 3.9%, respectively). However, the stability of the biodeposited Pd NPs was not satisfactory and the dihydrogen production decreased by 37% after five cycles. Addition of Nafion as binding agents therefore was needed to improve consistent catalytic performance (*98*).

Table 2. Nanocatalysts Synthesized by Bacteria and Their Applications

Nanocatalysts	*Bacteria*	*Applications*	*References*
Au	*S. oneidensis* MR-1	Biocatalysts	(*26*)
Cu	*S. oneidensis* MR-1	Biocatalysts	(*19*)
Pt	*S. oneidensis* MR-1	Biocatalysts	(*97*)
Pd	*S. oneidensis* MR-1	Electrocatalysts	(*34*, *98*)
		Biocatalysts	(*18*, *26*, *97*)
Se	*Lysinibacillus* sp. ZYM- 1	Photocatalysts	(*29*)
Te	*S. baltica*	Photocatalysts	(*96*)
Ag_2S	*S. oneidensis* MR-1	Photocatalysts	(*82*)
		Biocatalysts	(*20*)
FeS	*S. putrefaciens* CN32	Biocatalysts	(*85*)
CdS	*Moorella thermoacetica*	Biocatalysts	(*36*)
	S. oneidensis MR-1	Antibacterial agent	(*86*)
ZnS	*S. oneidensis* MR-1	Photocatalysts	(*99*)
PdAu	*S. oneidensis* MR-1	Electrocatalysts	(*17*)
		Biocatalysts	(*26*)
PdPt	*S. oneidensis* MR-1	Biocatalysts	(*97*)

The nanocatalysts synthesized by EAB are small and uniform but have poor crystallinity and conductivity, which may prevent electrocatalysis. Other subsequent treatments can be employed to improve the performance. A highly efficient electrocatalyst with a hybrid PdAu alloy covered with graphene oxide has been designed. The hybrid was initially synthesized by *S. oneidensis* MR-1 and underwent subsequent hydrothermal treatment. As shown in Figure 8, the hybrid showed a 6.15-fold higher mass electrocatalytic activity for ethanol oxidation in alkaline condition and a 6.58-fold higher activity for formate oxidation in acid condition compared to a commercial Pd/C catalyst with the same Pd loading of 4 μg cm^{-2} (*17*). The hybrid also showed better stability and continued outperforming the commercial Pd/C catalyst after 2000 s. The high catalytic activity was attributed to the three-dimensional porous structure and the carbon support as well as doping elements from *S. oneidensis* MR-1 cells, the nature of PdAu alloy, and the enhanced conductivity of reduced graphene oxide (*17*).

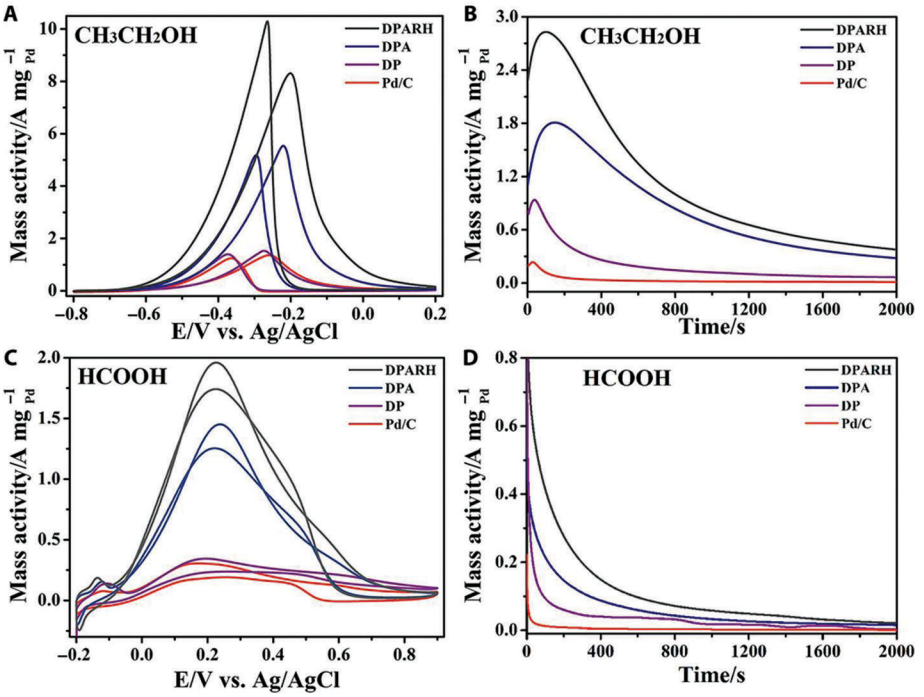

Figure 8. Electrocatalytic performances of as-prepared biogenic catalysts. (A) Cyclic voltammetry (CV) of the carbonized hybrids of S. oneidensis MR-1 cells, PdAu alloy with reduced graphene oxide (DPARH), carbonized hybrids of S. oneidensis MR-1 cells and PdAu alloy (DPA), carbonized hybrids of S. oneidensis MR-1 cells and Pd NPs (DP), and commercial Pd/C catalyst–modified electrodes in 1 M KOH + 1 M ethanol. Scan rate is 50 mV s^{-1}. Potentials versus Ag/AgCl (saturated KCl). (B) Chronoamperometric curves of the catalyst-modified electrodes in 1 M KOH + 1 M of ethanol at −0.3 V for 2000 s. (C) CVs of these catalyst-modified electrodes in 0.5 M H_2SO_4 + 0.5 M HCOOH. Scan rate is 50 mV s^{-1}. (D) Chronoamperometric curves of the catalyst-modified electrodes in 0.5 M of H_2SO_4 + 0.5 M HCOOH at 0.1 V for 2000 s. The Pd mass amounts of all the catalysts were about 1 μg in each electrode (17). Reproduced with permission from reference (17). Copyright 2016 by the American Association for the Advancement of Science.

Photocatalysis

The nanocatalysts formed on the EAB surface possess an ability to degrade pollutants that are resistant to biodegradation. As shown in Figure 9A, a hybrid of *S. oneidensis* MR-1 and 50 mg of biosynthesized ZnS NPs with a diameter of 5 nm totally degraded 20 mg L^{-1} of rhodamine B (RhB) in 3 h under UV irradiation. The 554-nm peak belonging to RhB vanished, and a new, blue-shifted peak (from 550 nm to 500 nm) appeared with the degradation, indicative of de-ethylation of the N,N,N′,N′-tetraethylrhodamine structure in RhB (Figure 9B). Further investigation concluded that the photogenerated holes generated by the biosynthesized ZnS, not the hydroxyl radicals, contributed to the photocatalysis (99).

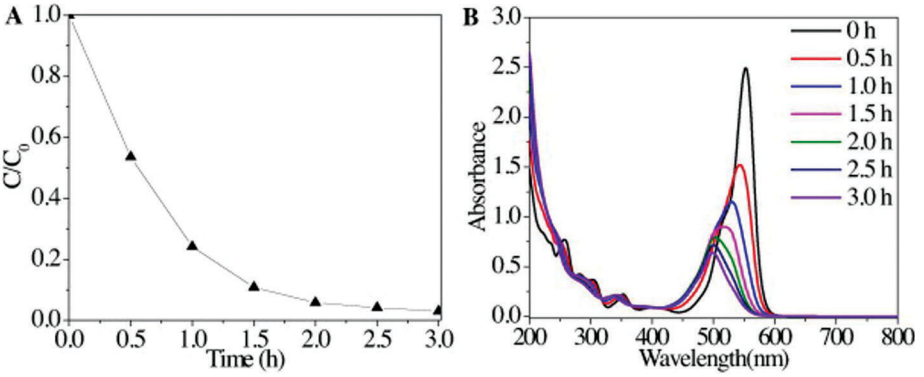

Figure 9. (A) Photocatalytic activity of synthesized ZnS nanocrystals for the photodegradation of rhodamine B (RhB) in aqueous solution (20 mg/L) in air. C_0 and C represent the initial concentration and residual concentrations of RhB, respectively. (B) UV-vis absorption changes of a RhB aqueous solution at room temperature in the presence of ZnS NPs under UV irradiation. Reproduced with permission from reference (99). Copyright 2015 Elsevier.

In a recent study, a mixture of chemically synthesized Ag_3PO_4 NPs and *S. oneidensis* MR-1 can degrade RhB with visible light irradiation under anaerobic conditions. After five days of light irradiation, 15 mg/L of RhB had been completely degraded by the Ag_3PO_4 NPs (0.5g/L) and *S. oneidensis* MR-1 cells. In this case, *S. oneidensis* MR-1 cells significantly enhanced the photocatalytic efficiency. As shown in Figure 10, the main role of *S. oneidensis* MR-1 was to provide electrons to the Ag_3PO_4 photocatalyst after Ag_3PO_4 excitation by light to produce photogenerated electrons in stepwise decomposition of RhB to rhodamine (*100*).

RhB can also be photodegraded by Se nanocatalysts synthesized by *Lysinibacillus* sp. ZYM-1 under visible light irradiation in combination with H_2O_2. *Lysinibacillus* sp. ZYM-1 produces Se nanorods, nanocubes, and nanospheres with different initial concentrations of selenite, but only the nanospheres showed photocatalytic performance. Ten milligrams of Se nanospheres photodecomposed RhB (10 mg L^{-1}, 50 mL) in 5 hours with a reaction rate constant of 0.0048 min^{-1} outperforming chemogenic Se nanomaterials. Both chromophore cleavage and N-de-ethylation contributed to the photodegradation (*29*).

The biogenic Ag_2S nanocatalysts produced by *S. oneidensis* MR-1 were also found to degrade pollutants under visible light irradiation. For example, coated on TiO_2 nanotubes, 20-mg Ag_2S nanocatalysts can photodecompose 4-nitrophenol (0.12 mmol L^{-1}, 50 mL) to 4-aminophenol completely within five hours. The photocatalytic activity increased with increasing molar ratio of Ag/Ti until 1/10, where the excess Ag_2S conglomerates and hinders the activity. One of the key factors is the electron transfer between Ag_2S NPs and TiO_2 nanotubes (*83*).

The reduction of methylene blue dye under sunlight is relatively slow, and only 20% reduction was detected after four hours. However, 90% reduction with 10 μg/mL Te NPs synthesized by *S. baltica* is achieved within the same period. Compared to the Te NPs obtained from chemical synthesis, the option of recycling is a notable advantage (*96*).

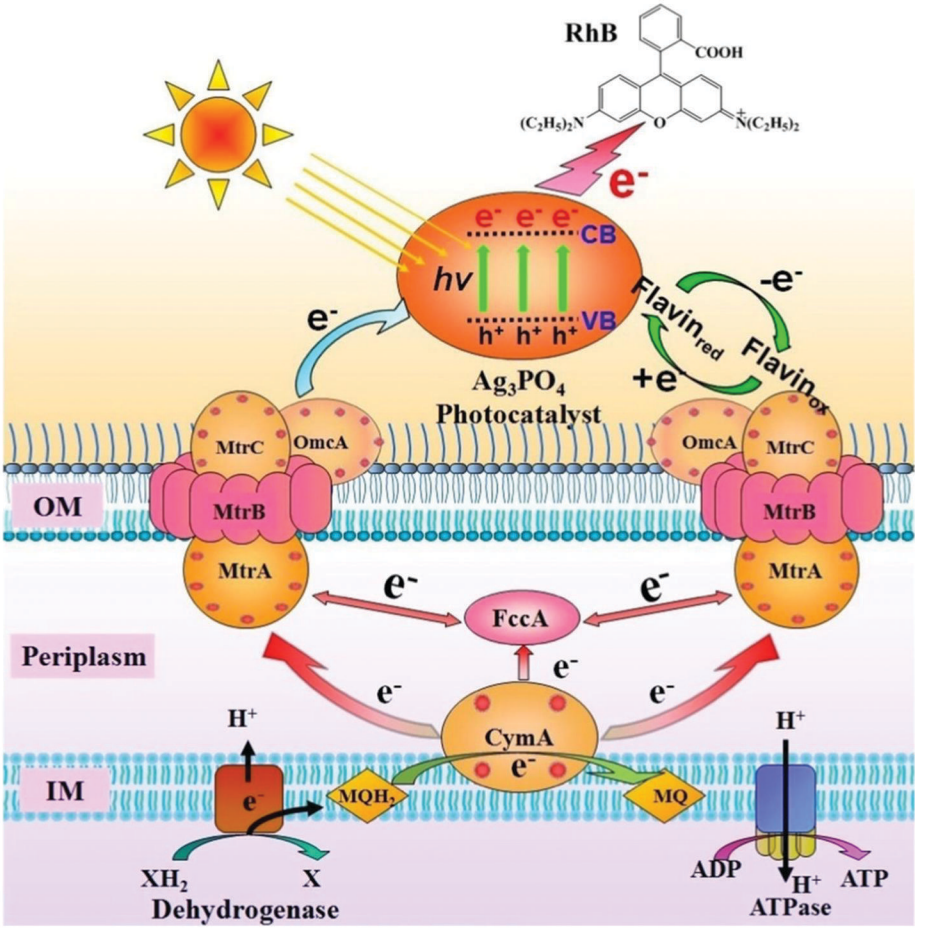

Figure 10. Proposed photocatalytic RhB degradation mechanisms in a biophotoelectric reductive degradation system. Arrows represent the electron flow. OM, outer membrane; IM, inner membrane. Adapted with permission from reference (*100*). *Copyright 2019 Elsevier.*

Biocatalysis

Biogenic Pd NPs also act as biocatalysts in other ways, such as in reductive dechlorination of polychlorinated biphenyls both in aqueous solution and in sediment matrices. Using formate as an electron donor, the hybrid of *S. oneidensis* MR-1 cells exposed to 500 mg/L of Pd(II) decomposed the polychlorinated 1 mg L^{-1} of 2,3,4-chlorobiphenyl to undetectable levels in 1 h at room temperature. The biocatalysis is enhanced when incubated in contaminated sediments. The hybrid from 50 mg/L of Pd(II) achieved dechlorination of seven polychlorinated biphenyls in 48 h, which is comparable to 500 mg/L of commercial Pd(0) powder (*18*).

Dechlorination of carbon tetrachloride was achieved using FeS biosynthesized by *S. putrefaciens* CN32. The hybrid of *S. putrefaciens* CN32 and biogenic FeS showed eight- and five-fold increases in dechlorination compared to *S. putrefaciens* CN32 and chemogenic FeS NPs, respectively. The efficient catalysis was attributed to the even distribution of FeS nanocatalysts and the larger amount of Fe(II) and disulfide. The addition of Fe(III) can enhance the catalytic efficiency further. The main role of *S. putrefaciens* CN32 is to produce FeS NPs that are well dispersed on the cell surface. The cell contribution is minimal after FeS formation (*85*).

The conventional method of biosynthesizing nanocatalysts is to retain the nanocatalyst coating on the cell membranes ("metallized" cells such as "palladized" cells) and ignore the non-cell-associated nanocatalysts in the bulk medium. However, one study showed that the extracellular nanocatalysts produced by *S. oneidensis* MR-1 outperformed the palladized cells. The initial rate of reduction of methyl viologen to methyl viologen cations radical of non-cell-associated Ag_2S (0.26 mM/s) is thus three-fold higher than that of cell-associated Ag_2S (0.26 mM/s). Another notable result is that the non-cell-associated Ag_2S from the mutant lacking OmcA and MtrC shows better performance than the wild-type strain (*20*). The morphology and structure of cell-associated nanocatalysts and non-cell-associated nanocatalysts may therefore not be identical, and equal attention should be given to these two kinds of nanocatalysts. Unlike chemogenic nanocatalysts, no additional capping agents or protecting agents are needed during biosynthesis due to the EPS secreted by the bacteria.

Photoautotrophic microorganisms can harvest light and carbon sources to produce food and energy. However, these processes are slow. On the other hand, although solid-state semiconductors can efficiently absorb light, semiconductors still face the challenge of converting photoexcited electrons into chemical bonds. Moreover, chemogenic semiconductors pose a threat to the environment during the synthesis process. A recent study combined the high efficiency of light harvesting by semiconductors with the low cost, self-replication, and self-repairing of the biology process. CdS NPs (<10 nm) were biodeposited on a nonphotosynthetic bacterium (*M. thermoacetica*) by incubating the bacteria in in a solution of Cd^{2+} and cysteine. The CdS NPs act as a photocatalyst and collect photons under light irradiation. The excited CdS NPs then deliver electrons to *M. thermoacetica*, which act as a biocatalyst and produce acetic acid from CO_2. The CdS NPs have three roles in the overall process: to harvest photons, to provide electrons, and to protect the bacteria from the damage caused by the light irradiation. High production of acetic acid was in fact harvested from this hybrid system over several days with light-dark cycles (*36*).

Outlook

In summary, biogenic nanocatalysts are small, well-dispersed, environmentally friendly, biocompatible, narrow-sized, and of low cost. In addition, some morphologies and properties are exclusive to biogenic nanocatalysts. However, there are also limitations on the biosynthesis of nanomaterials including nanocatalysts. Compared to their well-developed chemical synthesis counterparts, current biosynthesis of nanocatalysts are normally trial-and-error efforts, especially regarding morphology and structure control. The challenges of biosynthesis of nanocatalysts come from the complexity of biological processes. Different organisms, for example, bacteria, fungi, yeasts, and even plants, are able to achieve biosynthesis, but even for the same microorganisms, the processes proceed differently in different growth phases. The main contributing parts in biosynthesis are proteins, enzymes, polysaccharides, and specific functional groups in the cell membrane (such as carboxylate groups), most of which evolve during the lifetime of microbes. Another challenge is the scaling-up of the biosynthesis. Most biosynthesis is in the millimole scale, as a high concentration of metal ions can harm the microbes or inhibit the biosynthesis. Moreover, the biosynthesis of nanomaterials under mild temperature is time-consuming and unlikely to be accelerated by higher temperature and pressure as in chemical synthesis. The low concentration and relatively long synthesis time are bottlenecks for large-scale synthesis of biogenic nanocatalysts.

Considerable research efforts are needed to further explore the potential of biogenic nanocatalysts, with a focus on several key directions. First, the complete biosynthesis processes need

to be mapped in much greater detail, addressing, for example, whether or not metal ions pass through the outer cell membrane and which specific components of the microorganism (organelles, protein complexes, DNA) are key players in the biosynthesis. The answers to these questions offer clues to the synthesis sites of biogenic nanocatalysts, the constituents of the nanocatalysts, and the genes involved in the synthesis processes. Secondly, efforts should also be spent on exploring and designing applications for nanocatalysts. The main advantages of nanocatalyst synthesis and operations are mild experimental conditions, self-replication, and self-rehabilitation, but they are also fraught with low yields and long synthesis durations. A suitable application should make use of the advantages of biogenic nanocatalysts and avoid the disadvantages. Finally, subsequent treatments should be considered to overcome the shortcomings of biogenic nanocatalysts. Biosynthesis is therefore not the end of the synthesis process. Instead, the biogenic nanocatalysts act as precursors, and further processes should be mobilized to optimize the morphologies and structures of the nanocatalysts, aiming at better performance.

List of Abbreviations

AFM	Atomic force microscopy
CSAFM	Current-sensing atomic force microscopy
DP	Carbonized hybrids of *S. oneidensis* MR-1 cells and Pd NPs
DPA	Carbonized hybrids of *S. oneidensis* MR-1 cells and PdAu alloy
DPARH	Carbonized hybrids of *S. oneidensis* MR-1 cells, PdAu alloy with reduced graphene oxide
EAB	Electrochemically active bacteria
EDS	Energy-dispersive X-ray spectroscopy
EET	Extracellular electron transfer
EPS	Extracellular polymeric substances
HEPES	Sodium 4-(2-hydroxyethyl)-1-piperazineethanesulfonic acid
NP(s)	Nanoparticle(s)
PCB	Polychlorinated biphenyls
RhB	Rhodamine B
SEM	Scanning electron microscopy
STC	Small tetraheme cytochromeTEMTransmission electron microscopy
XPS	X-ray photoelectron spectroscopy
XRD	X-ray diffraction

Acknowledgments

Financial support from the China Scholarship Council (CSC) (No. 201606130019), Carlsberg Foundation (CF15-0164), the National Natural Science Foundation of China (41471260, 51478451), and Otto Mønsted Foundation is greatly appreciated.

References

1. ISO. *International Organization for Standardization. Nanotechnologies—vocabulary—part 1: Core Terms*; ISO/TS 80004-1; 2015.

2. Fu, Y.; Liang, F.; Tian, H.; Hu, J. Nonenzymatic Glucose Sensor Based on ITO Electrode Modified with Gold Nanoparticles by Ion Implantation. *Electrochim. Acta* **2014**, *120*, 314–318.
3. Jukk, K.; Kozlova, J.; Ritslaid, P.; Sammelselg, V.; Alexeyeva, N.; Tammeveski, K. Sputter-Deposited Pt Nanoparticle/Multi-Walled Carbon Nanotube Composite Catalyst for Oxygen Reduction Reaction. *J. Electroanal. Chem.* **2013**, *708*, 31–38.
4. Patel, N.; Fernandes, R.; Guella, G.; Kale, A.; Miotello, A.; Patton, B.; Zanchetta, C. Structured and Nanoparticle Assembled Co−B Thin Films Prepared by Pulsed Laser Deposition: A Very Efficient Catalyst for Hydrogen Production. *J. Phys. Chem. C* **2008**, *112*, 6968–6976.
5. Ariga, K.; Mori, T.; Hill, J. P. Mechanical Control of Nanomaterials and Nanosystems. *Adv. Mater.* **2012**, *24*, 158–176.
6. Xu, J.; Sun, J.; Wang, Y.; Sheng, J.; Wang, F.; Sun, M. Application of Iron Magnetic Nanoparticles in Protein Immobilization. *Molecules* **2014**, *19*, 11465–11486.
7. Gupta, S.; Kershaw, S. V.; Rogach, A. L. 25th Anniversary Article: Ion Exchange in Colloidal Nanocrystals. *Adv. Mater.* **2013**, *25*, 6923–6944.
8. Schwamborn, S.; Etienne, M.; Schuhmann, W. Local Electrocatalytic Induction of Sol–Gel Deposition at Pt Nanoparticles. *Electrochem. Commun.* **2011**, *13*, 759–762.
9. Zheng, Z.; Zheng, Y.; Tian, X.; Yang, Z.; Jiang, Y.; Zhao, F. Interactions Between Iron Mineral-Humic Complexes and Hexavalent Chromium and the Corresponding Bio-Effects. *Environ. Pollut.* **2018**, *241*, 265–271.
10. Cao, H.; Wang, X.; Gu, H.; Liu, J.; Luan, L.; Liu, W.; Wang, Y.; Guo, Z. Carbon Coated Manganese Monoxide Octahedron Negative-Electrode for Lithium-Ion Batteries with Enhanced Performance. *RSC Adv.* **2015**, *5*, 34566–34571.
11. Cao, H.; Wu, N.; Liu, Y.; Wang, S.; Du, W.; Liu, J. Facile Synthesis of Rod-Like Manganese Molybdate Crystallines with Two-Dimensional Nanoflakes for Supercapacitor Application. *Electrochim. Acta.* **2017**, *225*, 605–613.
12. Engelbrekt, C.; Sørensen, K. H.; Lübcke, T.; Zhang, J.; Li, Q.; Pan, C.; Bjerrum, N. J.; Ulstrup, J. 1.7 nm Platinum Nanoparticles: Synthesis with Glucose Starch, Characterization and Catalysis. *ChemPhysChem* **2010**, *11*, 2844–2853.
13. Engelbrekt, C.; Sorensen, K. H.; Zhang, J.; Welinder, A. C.; Jensen, P. S.; Ulstrup, J. Green Synthesis of Gold Nanoparticles with Starch-Glucose and Application in Bioelectrochemistry. *J. Mater. Chem.* **2009**, *19*, 7839–7847.
14. Hulkoti, N. I.; Taranath, T. C. Biosynthesis of Nanoparticles Using Microbes—A Review. *Colloids Surf., B* **2014**, *121*, 474–483.
15. Mohanpuria, P.; Rana, N. K.; Yadav, S. K. Biosynthesis of Nanoparticles: Technological Concepts and Future Applications. *J. Nanopart. Res.* **2008**, *10*, 507–517.
16. Roy, K.; Mao, H. Q.; Huang, S. K.; Leong, K. W. Oral Gene Delivery with Chitosan–DNA Nanoparticles Generates Immunologic Protection in a Murine Model of Peanut Allergy. *Nat. Med.* **1999**, *5*, 387–391.
17. Liu, J.; Zheng, Y.; Hong, Z.; Cai, K.; Zhao, F.; Han, H. Microbial Synthesis of Highly Dispersed Pdau Alloy for Enhanced Electrocatalysis. *Sci. Adv.* **2016**, *2*, e1600858.

18. Windt, W. D.; Aelterman, P.; Verstraete, W. Bioreductive Deposition of Palladium (0) Nanoparticles on *Shewanella oneidensis* with Catalytic Activity Towards Reductive Dechlorination of Polychlorinated Biphenyls. *Environ. Microbiol.* **2005**, *7*, 314–325.
19. Kimber, R. L.; Lewis, E. A.; Parmeggiani, F.; Smith, K.; Bagshaw, H.; Starborg, T.; Joshi, N.; Figueroa, A. I.; van der Laan, G.; Cibin, G.; Gianolio, D.; Haigh, S. J.; Pattrick, R. A. D.; Turner, N. J.; Lloyd, J. R. Biosynthesis and Characterization of Copper Nanoparticles Using *Shewanella oneidensis:* Application for Click Chemistry. *Small* **2018**, *14*, 1703145.
20. Ng, C. K.; Sivakumar, K.; Liu, X.; Madhaiyan, M.; Ji, L.; Yang, L.; Tang, C.; Song, H.; Kjelleberg, S.; Cao, B. Influence of Outer Membrane *c*-Type Cytochromes on Particle Size and Activity of Extracellular Nanoparticles Produced by *Shewanella oneidensis*. *Biotechnol. Bioeng.* **2013**, *110*, 1831–1837.
21. Li, D. B.; Cheng, Y. Y.; Wu, C.; Li, W. W.; Li, N.; Yang, Z. C.; Tong, Z. H.; Yu, H. Q. Selenite Reduction by *Shewanella oneidensis* MR-1 is Mediated by Fumarate Reductase in Periplasm. *Sci. Rep.* **2014**, *4*, 3735.
22. Ng, C. K.; Cai Tan, T. K.; Song, H.; Cao, B. Reductive Formation of Palladium Nanoparticles by *Shewanella oneidensis*: Role of Outer Membrane Cytochromes and Hydrogenases. *RSC Adv.* **2013**, *3*, 22498–22503.
23. Zhou, N. Q.; Tian, L. J.; Wang, Y. C.; Li, D. B.; Li, P. P.; Zhang, X.; Yu, H. Q. Extracellular Biosynthesis of Copper Sulfide Nanoparticles by *Shewanella oneidensis* MR-1 as a Photothermal Agent. *Enzyme Microb. Technol.* **2016**, *95*, 230–235.
24. Xiao, X.; Liu, Q. Y.; Lu, X. R.; Li, T. T.; Feng, X. L.; Li, Q.; Liu, Z. Y.; Feng, Y. J. Self-Assembly of Complex Hollow CuS Nano/Micro Shell by an Electrochemically Active Bacterium *Shewanella oneidensis* MR-1. *Int. Biodeterior. Biodegrad.* **2017**, *116*, 10–16.
25. Wu, R.; Cui, L.; Chen, L.; Wang, C.; Cao, C.; Sheng, G.; Yu, H.; Zhao, F. Effects of Bio-Au Nanoparticles on Electrochemical Activity of *Shewanella oneidensis* Wild Type and *ΔomcA/MtrC* Mutant. *Sci. Rep.* **2013**, *3*, 3307.
26. Tuo, Y.; Liu, G.; Dong, B.; Zhou, J.; Wang, A.; Wang, J.; Jin, R.; Lv, H.; Dou, Z.; Huang, W. Microbial Synthesis of Pd/Fe_3O_4, Au/Fe_3O_4 and PdAu/Fe_3O_4 Nanocomposites for Catalytic Reduction of Nitroaromatic Compounds. *Sci. Rep.* **2015**, *5*, 13515.
27. Miller, A.; Singh, L.; Wang, L.; Liu, H. Linking Internal Resistance with Design and Operation Decisions in Microbial Electrolysis Cells. *Environ. Int.* **2019**, *126*, 611–618.
28. Huang, B. C.; Yi, Y. C.; Chang, J. S.; Ng, I. S. Mechanism Study of Photo-Induced Gold Nanoparticles Formation by *Shewanella oneidensis* MR-1. *Sci. Rep.* **2019**, *9*, 7589.
29. Che, L.; Dong, Y.; Wu, M.; Zhao, Y.; Liu, L.; Zhou, H. Characterization of Selenite Reduction by *Lysinibacillus* sp. ZYM-1 and Photocatalytic Performance of Biogenic Selenium Nanospheres. *ACS Sustainable Chem. Eng.* **2017**, *5*, 2535–2543.
30. Søbjerg, L. S.; Gauthier, D.; Lindhardt, A. T.; Bunge, M.; Finster, K.; Meyer, R. L.; Skrydstrup, T. Bio-Supported Palladium Nanoparticles as a Catalyst for Suzuki–Miyaura and Mizoroki–Heck Reactions. *Green Chem.* **2009**, *11*, 2041–2046.
31. Gauthier, D.; Søbjerg, L. S.; Jensen, K. M.; Lindhardt, A. T.; Bunge, M.; Finster, K.; Meyer, R. L.; Skrydstrup, T. Environmentally Benign Recovery and Reactivation of Palladium from Industrial Waste by Using Gram-Negative Bacteria. *ChemSusChem* **2010**, *3*, 1036–1039.

32. Bunge, M.; Søbjerg, L. S.; Rotaru, A. E.; Gauthier, D.; Lindhardt, A. T.; Hause, G.; Finster, K.; Kingshott, P.; Skrydstrup, T.; Meyer, R. L. Formation of Palladium(0) Nanoparticles at Microbial Surfaces. *Biotechnol. Bioeng.* **2010**, *107*, 206–215.
33. Kowshik, M.; Vogel, W.; Urban, J.; Kulkarni, S. K.; Paknikar, K. M. Microbial Synthesis of Semiconductor PbS Nanocrystallites. *Adv. Mater.* **2002**, *14*, 815–818.
34. Wu, R.; Tian, X.; Xiao, Y.; Ulstrup, J.; Molager Christensen, H. E.; Zhao, F.; Zhang, J. Selective Electrocatalysis of Biofuel Molecular Oxidation Using Palladium Nanoparticles Generated on *Shewanella oneidensis* MR-1. *J. Mater. Chem. A* **2018**, *6*, 10655–10662.
35. Wang, T.; Yang, L.; Zhang, B.; Liu, J. Extracellular Biosynthesis and Transformation of Selenium Nanoparticles and Application in H_2O_2 Biosensor. *Colloids Surf., B* **2010**, *80*, 94–102.
36. Sakimoto, K. K.; Wong, A. B.; Yang, P. Self-Photosensitization of Nonphotosynthetic Bacteria for Solar-to-Chemical Production. *Science* **2016**, *351*, 74.
37. Zhang, H.; Liu, H.; Tian, Z.; Lu, D.; Yu, Y.; Cestellos-Blanco, S.; Sakimoto, K. K.; Yang, P. Bacteria Photosensitized by Intracellular Gold Nanoclusters for Solar Fuel Production. *Nat. Nanotechnol.* **2018**, *13*, 900–905.
38. Wu, R.; Wang, C.; Shen, J.; Zhao, F. A Role for Biosynthetic CdS Quantum Dots in Extracellular Electron Transfer of *Saccharomyces cerevisiae*. *Process Biochem.* **2015**, *50*, 2061–2065.
39. Beveridge, T. J.; Murray, R. G. Sites of Metal Deposition in the Cell Wall of *Bacillus subtilis*. *J. Bacteriol.* **1980**, *141*, 876–887.
40. Sweeney, R. Y.; Mao, C.; Gao, X.; Burt, J. L.; Belcher, A. M.; Georgiou, G.; Iverson, B. L. Bacterial Biosynthesis of Cadmium Sulfide Nanocrystals. *Chem. Biol.* **2004**, *11*, 1553–1559.
41. Derby, H.; Hammer, B. Bacteriology of Butter Iv. Bacteriological Studies on Surface Taint Butter. *Research Bulletin (Iowa Agriculture and Home Economics Experiment Station)* **1931**, *11*, 1.
42. MacDonell, M. T.; Colwell, R. R. Phylogeny of the Vibrionaceae, and Recommendation for Two New Genera, *Listonella* and *Shewanella*. *Syst. Appl. Microbiol.* **1985**, *6*, 171–182.
43. Myers, C. R.; Nealson, K. H. Bacterial Manganese Reduction and Growth with Manganese Oxide as the Sole Electron Acceptor. *Science* **1988**, *240*, 1319–1321.
44. Venkateswaran, K.; Moser, D. P.; Dollhopf, M. E.; Lies, D. P.; Saffarini, D. A.; MacGregor, B. J.; Ringelberg, D. B.; White, D. C.; Nishijima, M.; Sano, H.; Burghardt, J.; Stackebrandt, E.; Nealson, K. H. Polyphasic Taxonomy of the Genus *Shewanella* and Description of *Shewanella* oneidensis sp. Nov. *Int. J. Syst. Evol. Microbiol.* **1999**, *49*, 705–724.
45. Heidelberg, J. F.; Paulsen, I. T.; Nelson, K. E.; Gaidos, E. J.; Nelson, W. C.; Read, T. D.; Eisen, J. A.; Seshadri, R.; Ward, N.; Methe, B.; Clayton, R. A.; Meyer, T.; Tsapin, A.; Scott, J.; Beanan, M.; Brinkac, L.; Daugherty, S.; DeBoy, R. T.; Dodson, R. J.; Durkin, A. S.; Haft, D. H.; Kolonay, J. F.; Madupu, R.; Peterson, J. D.; Umayam, L. A.; White, O.; Wolf, A. M.; Vamathevan, J.; Weidman, J.; Impraim, M.; Lee, K.; Berry, K.; Lee, C.; Mueller, J.; Khouri, H.; Gill, J.; Utterback, T. R.; McDonald, L. A.; Feldblyum, T. V.; Smith, H. O.; Venter, J. C.; Nealson, K. H.; Fraser, C. M. Genome Sequence of the Dissimilatory Metal Ion–Reducing Bacterium *Shewanella oneidensis*. *Nat. Biotechnol.* **2002**, *20*, 1118–1123.
46. Suresh, A. K.; Pelletier, D. A.; Wang, W.; Moon, J. W.; Gu, B.; Mortensen, N. P.; Allison, D. P.; Joy, D. C.; Phelps, T. J.; Doktycz, M. J. Silver Nanocrystallites: Biofabrication Using

Shewanella oneidensis, and an Evaluation of Their Comparative Toxicity on Gram-Negative and Gram-Positive Bacteria. *Environ. Sci. Technol.* **2010**, *44*, 5210–5215.
47. Kumar, R.; Singh, L.; Wahid, Z. A.; Din, M. F. M. Exoelectrogens in Microbial Fuel Cells toward Bioelectricity Generation: A Review. *Int. J. Energy Res.* **2015**, *39*, 1048–1067.
48. Zheng, Z.; Xiao, Y.; Wu, R.; Mølager Christensen, H. E.; Zhao, F.; Zhang, J. Electrons Selective Uptake of a Metal-Reducing Bacterium *Shewanella oneidensis* MR-1 from Ferrocyanide. *Biosens. Bioelectron.* **2019**, *142*, 111571.
49. Xiao, Y.; Zhang, E.; Zhang, J.; Dai, Y.; Yang, Z.; Christensen, H. E. M.; Ulstrup, J.; Zhao, F. Extracellular Polymeric Substances Are Transient Media for Microbial Extracellular Electron Transfer. *Sci. Adv.* **2017**, *3*, e1700623.
50. Tian, X.; Zhao, F.; You, L.; Wu, X.; Zheng, Z.; Wu, R.; Jiang, Y.; Sun, S. Interaction between *in vivo* Bioluminescence and Extracellular Electron Transfer in *Shewanella woodyi* via Charge and Discharge. *Phys. Chem. Chem. Phys.* **2017**, *19*, 1746–1750.
51. El-Naggar, M. Y.; Wanger, G.; Leung, K. M.; Yuzvinsky, T. D.; Southam, G.; Yang, J.; Lau, W. M.; Nealson, K. H.; Gorby, Y. A. Electrical Transport Along Bacterial Nanowires from *Shewanella oneidensis* MR-1. *Proc. Natl. Acad. Sci. U. S. A.* **2010**, *107*, 18127–18131.
52. Marsili, E.; Baron, D. B.; Shikhare, I. D.; Coursolle, D.; Gralnick, J. A.; Bond, D. R. *Shewanella* Secretes Flavins that Mediate Extracellular Electron Transfer. *Proc. Natl. Acad. Sci. U. S. A.* **2008**, *105*, 3968–3973.
53. Mal, J.; Nancharaiah, Y. V.; van Hullebusch, E. D.; Lens, P. N. L. Metal Chalcogenide Quantum Dots: Biotechnological Synthesis and Applications. *RSC Adv.* **2016**, *6*, 41477–41495.
54. Park, T. J.; Lee, K. G.; Lee, S. Y. Advances in Microbial Biosynthesis of Metal Nanoparticles. *Appl. Microbiol. Biotechnol.* **2016**, *100*, 521–534.
55. Ghosh, S. Copper and Palladium Nanostructures: A Bacteriogenic Approach. *Appl. Microbiol. Biotechnol.* **2018**, *102*, 7693–7701.
56. Khatami, M.; Alijani, H. Q.; Sharifi, I. Biosynthesis of Bimetallic and Core–Shell Nanoparticles: Their Biomedical Applications – A Review. *IET Nanobiotechnol.* **2018**, *12*, 879–887.
57. Kim, T. Y.; Kim, M. G.; Lee, J. H.; Hur, H. G. Biosynthesis of Nanomaterials by *Shewanella* Species for Application in Lithium Ion Batteries. *Front. Microbiol.* **2018**, *9*, 2817.
58. Vaseghi, Z.; Nematollahzadeh, A.; Tavakoli, O. Green Methods for the Synthesis of Metal Nanoparticles Using Biogenic Reducing Agents: A Review. *Rev. Chem. Eng.* **2018**, *34*, 529.
59. Gahlawat, G.; Choudhury, A. R. A Review on the Biosynthesis of Metal and Metal Salt Nanoparticles by Microbes. *RSC Adv.* **2019**, *9*, 12944–12967.
60. Salunke, B. K.; Sawant, S. S.; Lee, S. I.; Kim, B. S. Microorganisms as Efficient Biosystem for the Synthesis of Metal Nanoparticles: Current Scenario and Future Possibilities. *World J. Microbiol. Biotechnol.* **2016**, *32*, 88.
61. van der Wal, A.; Minor, M.; Norde, W.; Zehnder, A. J. B.; Lyklema, J. Electrokinetic Potential of Bacterial Cells. *Langmuir* **1997**, *13*, 165–171.
62. Li, X.; Xu, H.; Chen, Z. S.; Chen, G. Biosynthesis of Nanoparticles by Microorganisms and Their Applications. *J. Nanomater.* **2011**, *2011*, 16.

63. Narayanan, K. B.; Sakthivel, N. Biological Synthesis of Metal Nanoparticles by Microbes. *Adv. Colloid Interface Sci.* **2010**, *156*, 1–13.
64. Beveridge, T. J. Role of Cellular Design in Bacterial Metal Accumulation and Mineralization. *Annu. Rev. Microbiol.* **1989**, *43*, 147–171.
65. Gorby, Y. A.; Yanina, S.; McLean, J. S.; Rosso, K. M.; Moyles, D.; Dohnalkova, A.; Beveridge, T. J.; Chang, I. S.; Kim, B. H.; Kim, K. S.; Culley, D. E.; Reed, S. B.; Romine, M. F.; Saffarini, D. A.; Hill, E. A.; Shi, L.; Elias, D. A.; Kennedy, D. W.; Pinchuk, G.; Watanabe, K.; Ishii, S. I.; Logan, B.; Nealson, K. H.; Fredrickson, J. K. Electrically Conductive Bacterial Nanowires Produced by *Shewanella oneidensis* Strain MR-1 and Other Microorganisms. *Proc. Natl. Acad. Sci. U. S. A.* **2006**, *103*, 11358–11363.
66. Kumar, R.; Singh, L.; Zularisam, A. W. Exoelectrogens: Recent Advances in Molecular Drivers Involved in Extracellular Electron Transfer and Strategies Used to Improve It for Microbial Fuel Cell Applications. *Renewable Sustainable Energy Rev.* **2016**, *56*, 1322–1336.
67. Shi, L.; Dong, H.; Reguera, G.; Beyenal, H.; Lu, A.; Liu, J.; Yu, H. Q.; Fredrickson, J. K. Extracellular Electron Transfer Mechanisms Between Microorganisms and Minerals. *Nat. Rev. Microbiol.* **2016**, *14*, 651–662.
68. Shi, L.; Squier, T. C.; Zachara, J. M.; Fredrickson, J. K. Respiration of Metal (Hydr)Oxides by *Shewanella* and *Geobacter*: A Key Role for Multihaem *C*-Type Cytochromes. *Mol. Microbiol.* **2007**, *65*, 12–20.
69. Kumar, A.; Hsu, L. H. H.; Kavanagh, P.; Barrière, F.; Lens, P. N. L.; Lapinsonnière, L.; Lienhard V, J. H.; Schröder, U.; Jiang, X.; Leech, D. The Ins and Outs of Microorganism–Electrode Electron Transfer Reactions. *Nat. Rev. Chem.* **2017**, *1*, 0024.
70. Belchik, S. M.; Kennedy, D. W.; Dohnalkova, A. C.; Wang, Y.; Sevinc, P. C.; Wu, H.; Lin, Y.; Lu, H. P.; Fredrickson, J. K.; Shi, L. Extracellular Reduction of Hexavalent Chromium by Cytochromes MtrC and OmcA of *Shewanella oneidensis* MR-1. *Appl. Environ. Microbiol.* **2011**, *77*, 4035.
71. Marshall, M. J.; Beliaev, A. S.; Dohnalkova, A. C.; Kennedy, D. W.; Shi, L.; Wang, Z.; Boyanov, M. I.; Lai, B.; Kemner, K. M.; McLean, J. S.; Reed, S. B.; Culley, D. E.; Bailey, V. L.; Simonson, C. J.; Saffarini, D. A.; Romine, M. F.; Zachara, J. M.; Fredrickson, J. K. *c*-Type Cytochrome-Dependent Formation of U(IV) Nanoparticles by *Shewanella oneidensis*. *PLoS Biol.* **2006**, *4*, 1324–1333.
72. Meshulam-Simon, G.; Behrens, S.; Choo, A. D.; Spormann, A. M. Hydrogen Metabolism in *Shewanella oneidensis* MR-1. *Appl. Environ. Microbiol.* **2007**, *73*, 1153–1165.
73. Kim, D. H.; Kanaly, R. A.; Hur, H. G. Biological Accumulation of Tellurium Nanorod Structures via Reduction of Tellurite by *Shewanella oneidensis* MR-1. *Bioresour. Technol.* **2012**, *125*, 127–131.
74. Klonowska, A.; Heulin, T.; Vermeglio, A. Selenite and Tellurite Reduction by *Shewanella oneidensis*. *Appl. Environ. Microbiol.* **2005**, *71*, 5607.
75. Xiao, Y.; Wu, S.; Zhang, F.; Wu, Y.; Yang, Z.; Zhao, F. Promoting Electrogenic Ability of Microbes with Negative Pressure. *J. Power Sources* **2013**, *229*, 79–83.
76. Wang, Z.; Zheng, Z.; Zheng, S.; Chen, S.; Zhao, F. Carbonized Textile with Free-Standing Threads as an Efficient Anode Material for Bioelectrochemical Systems. *J. Power Sources* **2015**, *287*, 269–275.

77. Perez-Gonzalez, T.; Jimenez-Lopez, C.; Neal, A. L.; Rull-Perez, F.; Rodriguez-Navarro, A.; Fernandez-Vivas, A.; Iañez-Pareja, E. Magnetite Biomineralization Induced by *Shewanella oneidensis*. *Geochim. Cosmochim. Acta* **2010**, *74*, 967–979.
78. Wu, X.; Zhao, F.; Rahunen, N.; Varcoe, J. R.; Avignone-Rossa, C.; Thumser, A. E.; Slade, R. C. T. A Role for Microbial Palladium Nanoparticles in Extracellular Electron Transfer. *Angew. Chem. Int. Ed.* **2010**, *50*, 427–430.
79. Konishi, Y.; Ohno, K.; Saitoh, N.; Nomura, T.; Nagamine, S.; Hishida, H.; Takahashi, Y.; Uruga, T. Bioreductive Deposition of Platinum Nanoparticles on the Bacterium *Shewanella algae*. *J. Biotechnol.* **2007**, *128*, 648–653.
80. Varia, J.; Zegeye, A.; Roy, S.; Yahaya, S.; Bull, S. *Shewanella putrefaciens* for the Remediation of Au^{3+}, Co^{2+} and Fe^{3+} Metal Ions from Aqueous Systems. *Biochem. Eng. J.* **2014**, *85*, 101–109.
81. Burns, J. L.; DiChristina, T. J. Anaerobic Respiration of Elemental Sulfur and Thiosulfate by *Shewanella oneidensis* MR-1 Requires *psrA*, a Homolog of the *phsA* Gene of *Salmonella enterica* Serovar Typhimurium LT2. *Appl. Environ. Microbiol.* **2009**, *75*, 5209–5217.
82. Voeikova, T. A.; Shebanova, A. S.; Ivanov, Y. D.; Kaysheva, A. L.; Novikova, L. M.; Zhuravliova, O. A.; Shumyantseva, V. V.; Shaitan, K. V.; Kirpichnikov, M. P.; Debabov, V. G. The Role of Proteins of the Outer Membrane of *Shewanella oneidensis* MR-1 in the Formation and Stabilization of Silver Sulfide Nanoparticles. *Appl. Biochem. Microbiol.* **2016**, *52*, 769–775.
83. Yang, M.; Shi, X. Biosynthesis of Ag_2s/Tio_2 Nanotubes Nanocomposites by *Shewanella oneidensis* MR-1 for the Catalytic Degradation of 4-Nitrophenol. *Environ. Sci. Pollut. Res.* **2019**, *26*, 12237–12246.
84. Butler, E. C.; Hayes, K. F. Effects of Solution Composition and Ph on the Reductive Dechlorination of Hexachloroethane by Iron Sulfide. *Environ. Sci. Technol.* **1998**, *32*, 1276–1284.
85. Huo, Y. C.; Li, W. W.; Chen, C. B.; Li, C. X.; Zeng, R.; Lau, T. C.; Huang, T. Y. Biogenic Fes Accelerates Reductive Dechlorination of Carbon Tetrachloride by *Shewanella putrefaciens* CN32. *Enzyme Microb. Technol.* **2016**, *95*, 236–241.
86. Wang, L.; Chen, S.; Ding, Y.; Zhu, Q.; Zhang, N.; Yu, S. Biofabrication of Morphology Improved Cadmium Sulfide Nanoparticles Using *Shewanella oneidensis* Bacterial Cells and Ionic Liquid: For Toxicity Against Brain Cancer Cell Lines. *J. Photochem. Photobiol., B* **2018**, *178*, 424–427.
87. Lee, J. H.; Kim, M. G.; Yoo, B.; Myung, N. V.; Maeng, J.; Lee, T.; Dohnalkova, A. C.; Fredrickson, J. K.; Sadowsky, M. J.; Hur, H. G. Biogenic Formation of Photoactive Arsenic-Sulfide Nanotubes by *Shewanella* sp. Strain HN-41. *Proc. Natl. Acad. Sci. U. S. A.* **2007**, *104*, 20410–20415.
88. Labrenz, M.; Druschel, G. K.; Thomsen-Ebert, T.; Gilbert, B.; Welch, S. A.; Kemner, K. M.; Logan, G. A.; Summons, R. E.; Stasio, G. D.; Bond, P. L.; Lai, B.; Kelly, S. D.; Banfield, J. F. Formation of Sphalerite (ZnS) Deposits in Natural Biofilms of Sulfate-Reducing Bacteria. *Science* **2000**, *290*, 1744–1747.
89. Lee, J.-H.; Kennedy, D. W.; Dohnalkova, A.; Moore, D. A.; Nachimuthu, P.; Reed, S. B.; Fredrickson, J. K. Manganese Sulfide Formation via Concomitant Microbial Manganese Oxide and Thiosulfate Reduction. *Environ. Microbiol.* **2011**, *13*, 3275–3288.

90. Lee, J. H.; Roh, Y.; Hur, H. G. Microbial Production and Characterization of Superparamagnetic Magnetite Nanoparticles by *Shewanella* sp. HN-41. *J. Microbiol. Biotechnol.* **2008**, *18*, 1572–1577.
91. Jiang, S.; Kim, M. G.; Kim, I. Y.; Hwang, S. J.; Hur, H. G. Biological Synthesis of Free-Standing Uniformed Goethite Nanowires by *Shewanella* sp. HN-41. *J. Mater. Chem. A* **2013**, *1*, 1646–1650.
92. Zannoni, D.; Borsetti, F.; Harrison, J. J.; Turner, R. J. The Bacterial Response to the Chalcogen Metalloids Se and Te. *Adv. Microb. Physiol.* **2007**, *53*, 1–312.
93. Tam, K.; Ho, C. T.; Lee, J. H.; Lai, M.; Chang, C. H.; Rheem, Y.; Chen, W.; Hur, H. G.; Myung, N. V. Growth Mechanism of Amorphous Selenium Nanoparticles Synthesized by *Shewanella* sp. HN-41. *Biosci. Biotechnol. Biochem.* **2010**, *74*, 696–700.
94. Pearce, C. I.; Pattrick, R. A. D.; Law, N.; Charnock, J. M.; Coker, V. S.; Fellowes, J. W.; Oremland, R. S.; Lloyd, J. R. Investigating Different Mechanisms for Biogenic Selenite Transformations: *Geobacter sulfurreducens*, *Shewanella oneidensis* and *Veillonella atypica*. *Environ. Technol.* **2009**, *30*, 1313–1326.
95. Kim, D. H.; Kim, M. G.; Jiang, S.; Lee, J. H.; Hur, H. G. Promoted Reduction of Tellurite and Formation of Extracellular Tellurium Nanorods by Concerted Reaction between Iron and *Shewanella oneidensis* MR-1. *Environ. Sci. Technol.* **2013**, *47*, 8709–8715.
96. Vaigankar, D. C.; Dubey, S. K.; Mujawar, S. Y.; D'Costa, A.; S. K, S. Tellurite Biotransformation and Detoxification by *Shewanella baltica* with Simultaneous Synthesis of Tellurium Nanorods Exhibiting Photo-Catalytic and Anti-Biofilm Activity. *Ecotoxicol. Environ. Saf.* **2018**, *165*, 516–526.
97. Tuo, Y.; Liu, G.; Dong, B.; Yu, H.; Zhou, J.; Wang, J.; Jin, R. Microbial Synthesis of Bimetallic PdPt Nanoparticles for Catalytic Reduction of 4-Nitrophenol. *Environ. Sci. Pollut. Res.* **2017**, *24*, 5249–5258.
98. Wang, W.; Zhang, B.; He, Z. Bioelectrochemical Deposition of Palladium Nanoparticles as Catalysts by *Shewanella oneidensis* MR-1 Towards Enhanced Hydrogen Production in Microbial Electrolysis Cells. *Electrochim. Acta* **2019**, *318*, 794–800.
99. Xiao, X.; Ma, X. B.; Yuan, H.; Liu, P. C.; Lei, Y. B.; Xu, H.; Du, D. L.; Sun, J. F.; Feng, Y. J. Photocatalytic Properties of Zinc Sulfide Nanocrystals Biofabricated by Metal-Reducing Bacterium *Shewanella oneidensis* MR-1. *J. Hazard. Mater.* **2015**, *288*, 134–139.
100. Xiao, X.; Ma, X. L.; Liu, Z. Y.; Li, W. W.; Yuan, H.; Ma, X. B.; Li, L. X.; Yu, H. Q. Degradation of Rhodamine B in a Novel Bio-Photoelectric Reductive System Composed of *Shewanella oneidensis* MR-1 and Ag_3PO_4. *Environ. Int.* **2019**, *126*, 560–567.